# Predictive modeling of a simple field matrix diffusion experiment addressing radionuclide transport in fractured rock. Is it so straightforward?

J. M. Soler [a*], I. Neretnieks [b], L. Moreno [b], L. Liu [b], S. Meng [b], U. Svensson [c], A. Iraola [d], H. Ebrahimi [d], P. Trinchero [d], J. Molinero [d], P. Vidstrand [e], G. Deissmann [f], J. Říha [g], M. Hokr [g], A. Vetešník [h], D. Vopálka [h], L. Gvoždík [i], M. Polák [i], D. Trpkošová [j], V. Havlová [j], D.-K. Park [k], S.-H. Ji [k], Y. Tachi [l], T. Ito [l], B. Gylling [m], G. W. Lanyon [n]

[a] IDAEA-CSIC, Barcelona, Spain

[b] KTH, Stockholm, Sweden

[c] CFE AB, Lyckeby, Sweden

[d] Amphos 21, Barcelona, Spain

[e] SKB, Solna, Sweden

[f] Forschungszentrum Jülich, Germany

[g] Technical University of Liberec, Czech Rep.

[h] Czech Technical University in Prague, Czech Rep.

[i] PROGEO, Roztoky, Czech Rep.

[j] ÚJV Řež, Czech Rep.

[k] KAERI, Daejeon, Rep. of Korea

[l] JAEA, Tokai, Japan

[m] Gylling GeoSolutions, Evanston, IL, USA

[n] Fracture Systems Ltd, St Ives, Cornwall, UK

[*] Corresponding author

Insititute of Environmental Assessment and Water Research (IDAEA-CSIC)

Jordi Girona 18-26, 08034 Barcelona, Catalonia, Spain

Tel: +34 934006100. E-mail: josep.soler@idaea.csic.es

## Abstract

The SKB GWFTS Task Force is an international forum in the area of conceptual and numerical modeling of groundwater flow and solute transport in fractured rock relevant for the deep geological disposal of radioactive waste. Two in situ matrix diffusion experiments in gneiss were performed at POSIVA's ONKALO underground facility in Finland. Synthetic groundwater containing several conservative and sorbing radiotracers was injected at one end of a borehole interval and flowed along a thin annulus towards the opposite end. Several teams performed predictive modeling of the tracer breakthrough curves using "conventional" modeling approaches (constant diffusion and sorption in the rock, no or minimum rock heterogeneity). Supporting information, derived from small-scale laboratory experiments, was provided. The teams were free to implement different concepts, use different codes and apply the transport and retention parameters that they considered to be most suited (i.e. not a benchmark exercise). The main goal was the comparison of the different sets of results and the analysis of the possible differences for this relatively simple experimental setup with a well-defined geometry.

The calculated peaks of the breakthrough curves were very sensitive to the assumed magnitude of dispersion in the borehole annulus. However, given the very different time scales for advection and matrix diffusion, the tails of the curves provided information concerning diffusion and retention in the rock matrix regardless of the magnitude of dispersion.

## Keywords

ONKALO, Fractured rocks, Matrix diffusion, Tracer tests, Numerical modeling

## Introduction

In the framework of the deep geological disposal of radioactive waste in fractured crystalline rocks, the diffusion of radionuclides from water-conducting fractures to the stagnant porewater of the adjacent wall rock, known as matrix diffusion, is the main retardation mechanism for the radionuclides once they may have eventually been released from their disposal canisters and surrounding engineering barriers (e.g. cementitious or compacted bentonite backfills). Numerous field and laboratory experiments studying matrix diffusion have been interpreted using mathematical solute transport models including advection and dispersion in the fractures and diffusion and retention (sorption) in the rock matrix.[1,2,3,4,5,6,7,8,9] However, the predictive capacity of these models is difficult to quantify, especially in relation to the concepts used in the models and their translation into effective transport and retention parameters. With this idea in mind, a purely predictive modeling exercise was designed within the SKB GWFTS Task Force (GroundWater Flow and Transport of Solutes, www.skb.se/taskforce). This Task Force is an international forum in the area of conceptual and numerical modeling of groundwater flow and solute transport in fractured rock. Task 9 within the Task Force addresses the modeling of coupled matrix diffusion and sorption in heterogeneous crystalline rock matrix at depth, which is performed in the context of in situ diffusion experiments at the ONKALO underground rock research facility (Finland) and at the Äspö Hard Rock Laboratory (Sweden). The modeling exercise described here (Task 9A) was designed for modeling teams to make predictive calculations of tracer breakthrough curves in the Water Phase Diffusion Experiments (WPDE)[10,11] at ONKALO. These were field solute transport experiments in veined gneiss subject to a simple well-characterized geometry. Synthetic groundwater containing several conservative and sorbing radiotracers (tracer pulses) was injected at one end of a borehole interval (Fig. 1). HTO, $^{36}Cl$ and $^{22}Na$ were used as tracers in both experiments. Additionally, $^{85}Sr$ and $^{133}Ba$ were

injected in WPDE-2. Water flowed along the annulus (slot aperture 1.25 mm) between an inner polyether ether ketone (PEEK) dummy and the borehole wall, simulating an open fracture in the rock. Tracers were able to diffuse into and out of the rock matrix around the borehole. Flow rates were 20.1 μL/min (WPDE-1) and 10.0 μL/min (WPDE-2). The main goal of this modeling exercise was the comparison of different predictive calculations and the analysis of the possible differences between the different sets of results. The discussion of the experimental results and their interpretation[10,11] were not part of the modeling exercise and are not addressed here. However, for the sake of completeness, the measured breakthrough curves are also reported and compared with the predictions.

The experimental setup, flow rates, injected tracer activities and rock mineralogies were provided in the task description[12] (downloadable from www.skb.se), together with available supporting experimental data concerning rock properties (porosities, effective diffusion coefficients, capacity factors, batch sorption distribution coefficients; see supplemental material). The modeling teams were asked to make predictions of the tracer breakthrough curves, based on the supplied information. The different teams were free to formulate their own concepts and use the transport and retention parameters that they considered to be most suited to the experiment (i.e. not a benchmarking exercise). They were also asked to consider relatively simple conventional models (traditional advection-dispersion in the borehole annulus, Fickian diffusion and constant sorption distribution coefficients in the rock matrix, homogeneous rock properties), although more complex models could be used when providing alternative results. In addition to a central prediction, upper and lower bounds for the breakthrough curves were to be provided, based mainly on parameter uncertainty.

Details of all the model calculations performed by the different teams are available in SKB Report R-17-10[13] (downloadable from www.skb.se). Here the goal is to provide an overview of the modeling concepts, the main results and the key conclusions from the study.

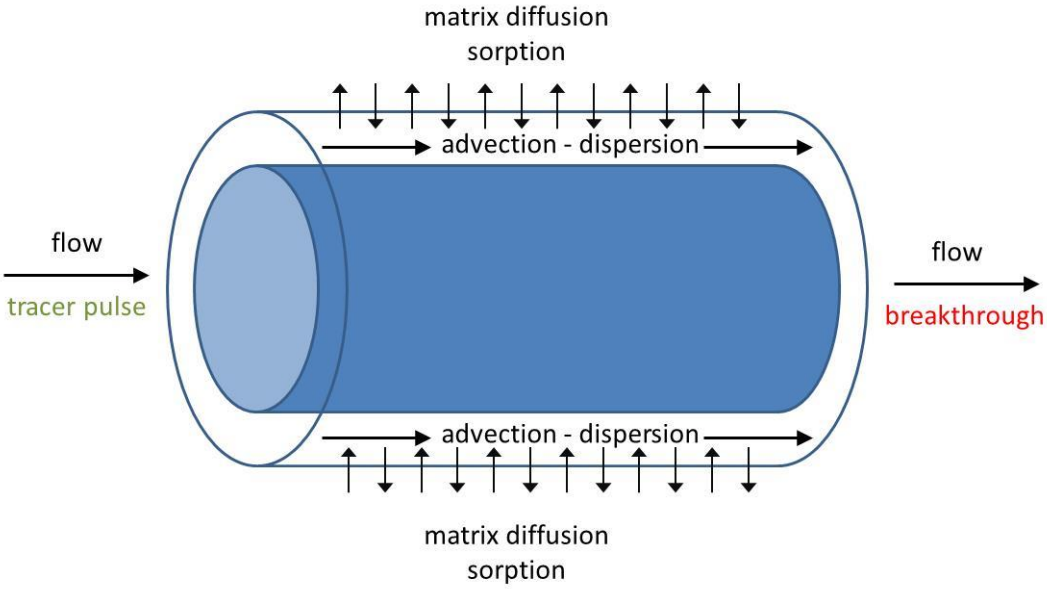


Fig. 1. Concept of the Water Phase Diffusion Experiments (WPDE). Water (continuous) and tracers (pulse) were injected at one end of the borehole interval. Water flowed along the annulus around an inner PEEK dummy (blue) and was sampled at the other end of the interval. The length and outer diameter of the interval were 1.905 m and 56.5 mm, respectively. The annulus had an aperture of 1.25 mm.

**Models and parameters**

Nine different modeling teams participated in Task 9A. However, issues in the implementation of rock capacity (combined effect of porosity and sorption) in one of the codes resulted in anomalous results. These results will not be presented here.

All models solved the advection-dispersion equation, which describes the conservation of solute mass subject to transport by advection and dispersion. The equation can be written as

$$\frac{\partial C_{tot}}{\partial t} = \nabla \cdot (\mathbf{D} \nabla C) - \nabla \cdot (\mathbf{q} C) \qquad (1)$$

where $C_{tot}$ is the total solute concentration (mass per volume of solution, e.g. mol/m$^3$ or Bq/m$^3$, including the sorbed fraction), $C$ is concentration in solution (mass per volume of solution), $t$ is time (s), **D** is the combined dispersion-diffusion tensor (m$^2$/s) and **q** is the Darcy velocity (m$^3$/m$^2$/s). $C_{tot}$ is given by

$$C_{tot} = \varepsilon C + \rho_d K_d C = \alpha C \quad (2)$$

where $\varepsilon$ is porosity, $\rho_d$ is the bulk dry density of the rock (kg/m$^3$), $K_d$ is the linear sorption distribution coefficient (m$^3$/kg) and $\alpha$ is the rock capacity factor ($\alpha = \varepsilon + \rho_d K_d$). The **D** tensor is the sum of the mechanical dispersion $\mathbf{D_d}$ and the effective diffusion coefficient $\mathbf{D_e}$. $\mathbf{D_d}$ can be written as

$$\mathbf{D_{d,ij}} = \alpha_T |q| + (\alpha_L - \alpha_T) \frac{q_i q_j}{|q|} \quad (3)$$

where $\alpha_T$ and $\alpha_L$ are the transverse and longitudinal dispersivities (m) and $q$ is the magnitude of the Darcy velocity. In this formulation it is assumed that that the principal direction of flow is aligned with the numerical grid.

In the numerical models, all external boundaries were subject to no-flux conditions, except where water flowed into or out of the domain (inlet and outlet of the borehole annulus). Advective flux conditions (solute flux $J_{solute}$ = **q**C) were implemented at those points. For the model implementing an analytical solution, zero concentration at infinite distance from the annulus into the rock matrix was assumed. Concerning the initial conditions, no tracer was initially present in the domain. Tracers were injected by advection, at a given constant concentration, during a specified time (pulse injection). In all the cases, water flow and advection was restricted to the borehole annulus. Solute transport in the rock matrix was only by diffusion, which was isotropic in all the calculations.

Below is a summary of the different models. Further details can be found in SKB Report R-17-10[13]. The term radial in the descriptions below refers to cylindrical

symmetry around the borehole axis. Notice that some teams only considered the dominant lithology along the borehole (veined gneiss), while other teams also considered the small amount of pegmatitic granite also present (veined gneiss from 0 to 0.35 m and from 0.5 m to 1.905 m along the borehole section; pegmatitic granite between 0.35 m and 0.5 m).

**Royal Institute of Technology (KTH).** Analytical solution (2D linear).

The model described advection and dispersion (AD) in the narrow slot coupled to matrix diffusion (MD). Matrix diffusion was modeled as being linear instead of radial due to the small transport distances involved. Dispersion was accounted for as Taylor dispersion in the slot (reflecting faster flow velocities in the center of the annulus) as well as in the inlet and outlet tubes. To avoid numerical difficulties, the AD equation was solved setting dispersion equal to zero. Then a simple analytical solution for A+MD was available for linear MD. In order to account for the neglected Taylor dispersion in the slot in the AD model, the dispersion was modeled as velocity dispersion (VD) with the same variance in the residence times of the solutes. The VD in principle describes a bundle of streamlines, mixed at the outlet, in which the residence time distribution is modeled with the A+MD model with a distribution of water residence times ($t_w$). The $t_w$ distribution was chosen such that the resulting Peclet number was the same as that due to Taylor dispersion.

**Japan Atomic Energy Agency (JAEA).** Continuum model (2D radial), including a Borehole Disturbed Zone (1 mm). GoldSim code.[14]

Radionuclide transport in the experimental borehole section was modeled taking into account advection and Fickian dispersion in the water-filled annular slot between the borehole wall and the inner PEEK dummy, together with diffusion and sorption in the surrounding rock matrix. One-dimensional flow was assumed for treating advection and dispersion in the slot. The dispersion effect caused by variations in flow velocity was

expressed by a dispersion coefficient. Matrix diffusion and sorption were modeled assuming a homogeneous rock matrix. However, a thin Borehole Disturbed Zone (BDZ) with different diffusion and sorption properties was considered.

**Technical University of Liberec (TUL).** Mixed continuum-fracture model, 2D fracture + 3D rock (full 360° section normal to the flow direction). Flow123d code.[15]

The calculations considered homogeneous advection and Fickian dispersion in the slot together with diffusion and sorption in the rock matrix. However, the 3D rock matrix was divided into three volumes to explicitly differentiate the two different rock types found along the experimental borehole: veined gneiss 1 (0 - 0.35 m along the borehole axis), pegmatitic granite (0.35 – 0.5 m) and veined gneiss 2 (0.5 – 1.905 m). Each section of rock matrix was considered to be homogeneous.

**PROGEO.** Continuum model (2D radial). MT3DMS code.[16]

The modeling approach and setup were equivalent to those used by TUL, but using a 2D radial numerical domain instead of a full 3D model.

**ÚJV ŘEŽ, A.S. (UJV).** Continuum model (2D radial). GoldSim code.[14]

The modeling approach and setup were also equivalent to those used by TUL, but using a 2D radial numerical domain instead of a full 3D model.

**Czech Technical University in Prague (CTU).** Continuum model (2D radial). GoldSim code.[14]

As in the case of PROGEO and UJV, the modeling approach and setup were equivalent to those used by TUL, but using a 2D radial numerical domain instead of a full 3D model.

**AMPHOS 21 (A21).** Continuum model (2D radial). PFLOTRAN code.[17]

The calculations considered advection and Fickian dispersion in the slot together with diffusion and sorption in a homogeneous rock matrix of limited thickness (1.8 cm). The

thin matrix allowed the successful comparison with results from an additional 3D model of restricted size (not presented hee).

**Korea Atomic Energy Research Institute (KAERI).** Continuum model (3D, 22.5° section normal to the flow direction). COMSOL Multiphysics code.[18,19]

The calculations considered homogeneous advection and Fickian dispersion in the slot together with diffusion and sorption in a homogeneous rock matrix.

Table 1 shows a compilation of parameters used in the different modeling exercises (central cases). In principle, the teams from the Czech Republic (UJV, TUL, CTU, PROGEO) had agreed to use the same parameter values, except for the thickness of the matrix. However, due to issues during the implementation of those values in the code, UJV ended up using smaller porosities. These teams also considered the two different lithologies (veined gneiss - VGN, 92.1% of the interval length, and pegmatitic granite - PGR, 7.9% of the length) surrounding the borehole, while the rest of the teams only considered the dominant lithology (VGN). JAEA assumed the presence of a BDZ with a thickness of 1 mm and increased diffusion coefficients, porosities and distribution coefficients. The assumption was that parameter values measured in the laboratory were applicable to the BDZ, while smaller values applied to the rest of the rock matrix (in situ conditions). In addition, A21 and JAEA did not consider the time spent by the tracers in the inlet and outlet tubing of the experiment. Mean residence times of water in the experimental slot (1.905 m in length), defined as volume of the slot divided by the volumetric flow rate, were 343 h (WPDE-1) and 689 h (WPDE-2). The additional times in the tubing, from the tracer vials to the sampling point, were 35.5 h (WPDE-1) and 71.3 h (WPDE-2).

Overall, the porosities, diffusion coefficients and distribution coefficients used by the different teams were rather similar (aside from the smaller porosities finally implemented by UJV). Notice that the VGN lithology dominates the composition of the rock matrix in the models used by the Czech groups. Exceptions are the large $^{36}Cl$ porosities used by JAEA and KAERI (they used the same values as for HTO) and the large $^{36}Cl$ diffusion coefficient used by JAEA. The $^{36}Cl$ diffusion coefficients and accessible porosities for PGR (7.9% of the interval length) used by the Czech groups were also very large, based on a single set of reported values for that lithology ($D_e = 5\times10^{-13}$ $m^2/s$, $\varepsilon = 0.013$; Table S2 in the supplemental material; task description[12]).

Results were to be provided as activity flow normalized to the total injected activity ((Bq/h)/Bq). Activities were also to be corrected for radioactive decay to the start of tracer injection ($t = 0$). Since only cases without sorption or with linear sorption were considered, decay correction was achieved by simply not including radioactive decay in the calculations.

Table 1. Parameters used by the different modeling teams (central cases).

| **Team** | **Matrix thickness** (cm) | $\rho_d$ (kg/m$^3$) | $D_e$**(HTO)** (×10$^{-13}$ m$^2$/s) | $\varepsilon$**(HTO)** | $D_e$**(Cl)** (×10$^{-15}$ m$^2$/s) | $\varepsilon$**(Cl)** | $D_e$**(Na)** (×10$^{-13}$ m$^2$/s) | $\varepsilon$**(Na)** | $K_d$**(Na)** (×10$^{-3}$ m$^3$/kg) | $D_e$**(Sr)** (×10$^{-13}$ m$^2$/s) | $\varepsilon$**(Sr)** | $K_d$**(Sr)** (×10$^{-3}$ m$^3$/kg) | $D_e$**(Ba)** (×10$^{-13}$ m$^2$/s) | $\varepsilon$**(Ba)** | $K_d$**(Ba)** (×10$^{-2}$ m$^3$/kg) | **Dispersion** $D_d$ (m$^2$/s) or $\alpha_L$ (m) |
|---|---|---|---|---|---|---|---|---|---|---|---|---|---|---|---|---|
| KTH | Infinite | 2650 | 2.00 | 0.01 | 5.0 | 0.000175 | 2.00 | 0.01 | 1.0 | 2.0 | 0.01 | 1.1 | 2.00 | 0.01 | 7.0 | 2×10$^{-9}$ m$^2$/s |
| A21 | 1.8 | 2750 | 2.50 | 0.01 | 5.0 | 0.0002 | 2.50 | 0.01 | 1.3 | 2.5 | 0.01 | 1.1 | 2.50 | 0.01 | 6.0 | 0.001 m |
| JAEA (matrix) | 20 | 2740 | 1.80 | 0.0063 | 150 | 0.0063 | 2.10 | 0.0063 | 1.1 | 2.5 | 0.0063 | 0.59 | 2.50 | 0.0063 | 2.5 | 0.045 m |
| JAEA (BDZ) | 20 | 2740 | 4.30 | 0.0097 | 350 | 0.0097 | 5.20 | 0.0097 | 1.3 | 6.0 | 0.0097 | 1.1 | 6.00 | 0.0097 | 6.0 | 0.045 m |
| TUL (VGN) | 10 | 2700 | 1.83 | 0.0082 | 5.0 | 0.000175 | 4.65 | 0.0082 | 1.3 | 3.3 | 0.0082 | 1.1 | 1.47 | 0.0082 | 6.0 | 0.19 m |
| TUL (PGR) | 10 | 2700 | 5.70 | 0.005 | 500 | 0.013 | 4.65 | 0.005 | 0.8 | 3.3 | 0.005 | 1.1 | 1.47 | 0.005 | 8.0 | 0.19 m |
| UJV (VGN) | 100 | 2700 | 1.83 | 0.0004 | 5.0 | 4.4×10$^{-5}$ | 4.65 | 0.0017 | 1.3 | 3.3 | 0.0021 | 1.1 | 1.47 | 0.0014 | 6.0 | 0.19 m |
| UJV (PGR) | 100 | 2700 | 5.70 | 0.0014 | 500 | 0.0010 | 4.65 | 0.0020 | 0.8 | 3.3 | 0.0024 | 1.1 | 1.47 | 0.0016 | 8.0 | 0.19 m |
| CTU (VGN) | 28 (2 for $^{133}$Ba) | 2700 | 1.83 | 0.0082 | 5.0 | 0.000175 | 4.65 | 0.0082 | 1.3 | 3.3 | 0.0082 | 1.1 | 1.47 | 0.0082 | 6.0 | 0.19 m |
| CTU (PGR) | 28 (2 for $^{133}$Ba) | 2700 | 5.70 | 0.005 | 500 | 0.013 | 4.65 | 0.005 | 0.8 | 3.3 | 0.005 | 1.1 | 1.47 | 0.005 | 8.0 | 0.19 m |
| PROGEO (VGN) | 20 | 2700 | 1.83 | 0.0082 | 5.0 | 0.000175 | 4.65 | 0.0082 | 1.3 | -- | ---- | -- | ---- | ---- | -- | 0.20 m |
| PROGEO (PGR) | 20 | 2700 | 5.70 | 0.005 | 500 | 0.013 | 4.65 | 0.005 | 0.8 | -- | ---- | -- | ---- | ---- | -- | 0.20 m |
| KAERI | 7.2 | 2700 | 2.50 | 0.0063 | 5.0 | 0.0063 | 4.65 | 0.0063 | 1.26 | 3.3 | 0.0063 | 1.1 | 1.47 | 0.0063 | 6.16 | 0.19 m |

$\rho_d$: bulk dry density. $D_e$: Effective diffusion coefficient. $\varepsilon$: Porosity. $K_d$: Distribution coefficient. $D_d$: Dispersion coefficient. $\alpha_L$: Longitudinal dispersivity. The dispersion coefficient used by KTH is equivalent to dispersivities of 2.6×10$^{-3}$ m (WPDE-1) and 5.3×10$^{-3}$ m (WPDE-2).

## Results and discussion

### *WPDE-1 (central cases)*

*HTO*

Figure 2 shows the calculated breakthrough curves (normalized decay-corrected activity flow NDCAF vs. time) for HTO. The most striking feature is the difference between the results from the teams assuming very small dispersivities (KTH, A21) and the results from the rest of the teams, who considered larger dispersivities (ranging from 0.045 m to 0.20 m). Small dispersivities result in tall and narrow breakthrough curves with very sharp arrivals, while larger dispersivities result in much shorter and wider curves with very early first arrivals (much earlier than the mean residence time of water in the borehole slot). JAEA assumed an intermediate value of dispersivity in the slot (0.045 m), compared to the values of 0.19 – 0.20 m (ca. 10% of the path length) used by other teams. The effect can be readily seen from the results.

When looking at the results in a log-log scale (Fig. 2b), the main peak is dominated by advection-dispersion in the slot, while the tail is controlled by out-diffusion from the rock matrix to the water flowing in the slot. The typical slope of the tail in a log-log plot, when matrix diffusion is not limited by the thickness of the rock matrix, and for linear diffusion orthogonal to the direction of flow, is -1.5.[Refs.1,20,21] The different values of dispersivity affect solute transport in the slot, where water flow takes place, and affect the shape and height of the main peak. However, since the characteristic time scales for advection (hundreds of hours) and matrix diffusion (thousands of hours) are very different, it has been shown[22] that the two parts of the curve are indeed decoupled and the tail reflects the diffusion and retention properties of the rock matrix regardless of the effect of dispersivity on the main peak.

(a)

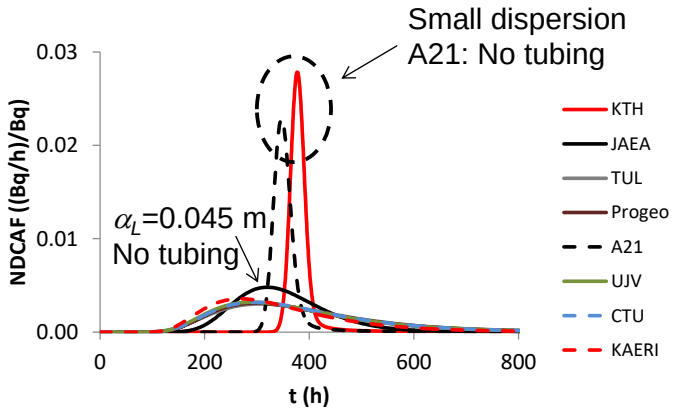


(b)

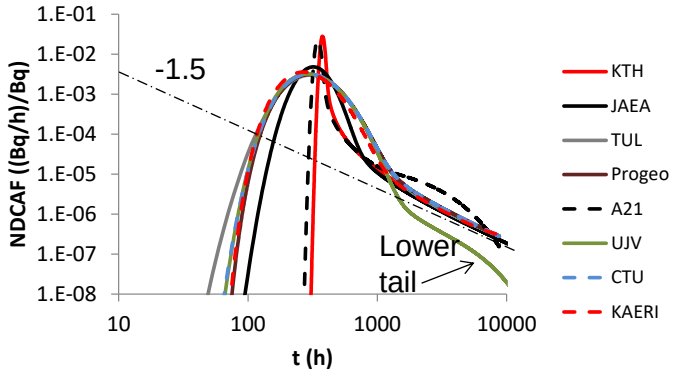


Fig. 2 WPDE-1 model results for HTO (NDCAF vs. time). (a) linear – linear scale, (b) log – log scale (a line with a slope of -1.5 is shown for reference).

Looking first at the main peak (Fig. 2), the difference in the position of the peaks between the results from A21 and KTH, both using small dispersivities, is due to the fact that A21 did not consider the time spent by the tracer in the tubing at the inlet and outlet of the experimental borehole interval. Different peak heights are also clearly observed between the results from the teams using small dispersivities (A21, KTH) and those from the rest. The intermediate value of dispersivity used by JAEA (0.045 m) is also reflected in the results. The small differences in the first arrival times between the different Czech teams and also KAERI (Fig. 2b) are due to numerical reasons, i.e. differences in the spatial and temporal discretizations implemented in the models.

Concerning the tails of the breakthrough curves, they are basically identical, reflecting also the characteristic -1.5 slope, except for those from A21 and UJV. The tail from A21 shows an initial flattening of the slope shortly after the peak and a pronounced drop in activity starting at about $t$ = 4000 h (Fig. 2b). From analytical solutions for planar fracture geometries,[23,24] matrix thickness should only affect the slope of the tail of the breakthrough curve and not its level. Figure 3 shows results of calculations performed with the CrunchFlow code.[25,26] The parameters of the calculations are the same as those used by the Czech TUL, PROGEO and CTU groups, but considering only veined gneiss (VGN) as the rock type around the borehole. The different breakthrough curves are for different matrix thicknesses (100, 10, 1.75 cm); different geometries (cylindrical – 2D radial and rectangular – 2D linear) are also compared for the largest matrix thickness. The results show that matrix thickness only has an effect if a very thin matrix is considered. The tail from A21 clearly shows an effect from the very limited matrix thickness that was considered (1.8 cm). Concerning the possible difference between cylindrical and rectangular geometries, this difference should be more evident for the case of a very thick matrix. However, the results show no effect, due to the thin (< 10 cm) diffusion profiles in the rock matrix in the calculations.

Regarding the lower level of the tail corresponding to the results from UJV, this lower level is due to the smaller porosities that were implemented by UJV compared to those used by the other teams (Table 1). As shown in the literature,[21,27] the level of the tail is proportional to the square root of $D_e\varepsilon$ (conservative tracers) or $D_e\alpha$ (sorbing tracers), where $\alpha$ is the rock capacity factor ($\alpha = \varepsilon + \rho_d K_d$).

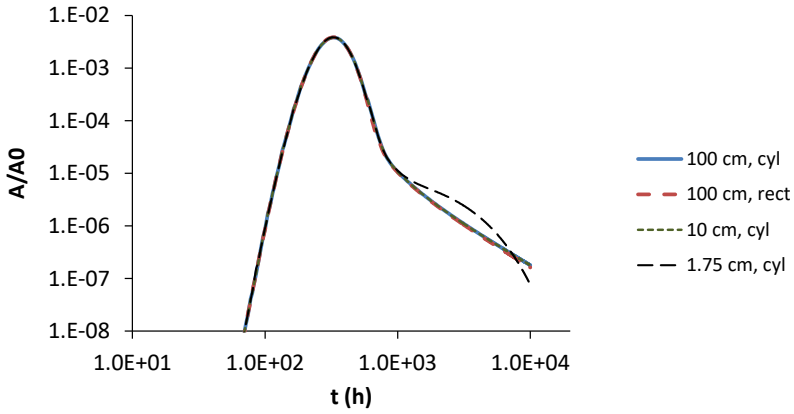


Fig. 3. WPDE-1 model results for HTO (relative activities A/A0 vs. time) using CrunchFlow. Tubing (inlet and outlet) is not included in the calculation. Results are for different matrix thicknesses (100, 10, 1.75 cm) and geometries (cylindrical - 2D radial and rectangular - 2D linear).

### *$^{36}Cl$*

Figure 4 shows the calculated breakthrough curves (NDCAF vs. time) for $^{36}$Cl. As in the case of HTO, the most striking feature is the difference between the results from the teams assuming very small dispersivities (KTH, A21) and the results from the rest of the teams. JAEA used an intermediate value of dispersivity (0.045 m).

Concerning the tails of the breakthrough curves, the results (Fig. 4b) show the low activities in the tail from UJV (compare UJV vs. TUL-PROGEO-CTU), similar to those for HTO. UJV implemented smaller porosities compared to the rest of the Czech teams (Table 1), which explains this lower tail. JAEA used $D_e$ and $\varepsilon$ values very similar to those for HTO, explaining also the high level of its corresponding tail.

(a)

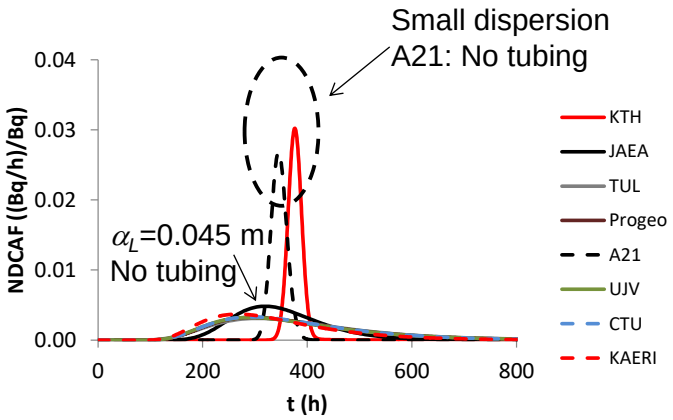


(b)

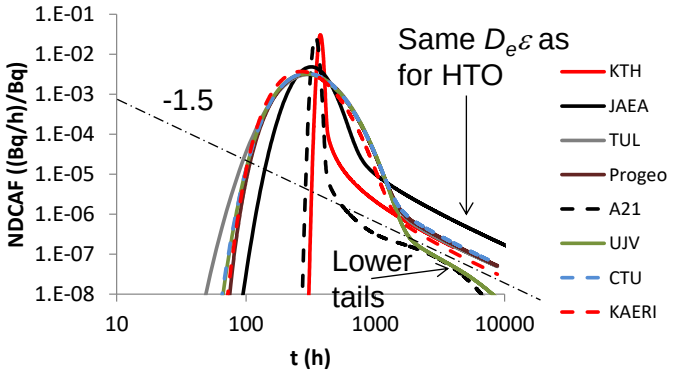


Fig. 4. WPDE-1 model results for $^{36}$Cl (NDCAF vs. time). (a) linear – linear scale, (b) log – log scale (a line with a slope of -1.5 is shown for reference).

The tails of the curves from KTH and A21 should be practically the same (practically equal $D_e$ and ε values), but the levels are clearly different. This difference is most probably caused by the implementation of numerical parameter values slightly different from those intended. A porosity value similar to that for HTO was probably implemented by KTH. Notice that the level of these tails should be lower than that from KAERI, which used the same value of $D_e$ but a larger porosity. Concerning the effect of matrix thickness, the breakthrough curve from A21 shows a drop in activity starting at about 2000 h due to the thin matrix considered in that model (1.8 cm).

$^{22}Na$

A quick inspection of the results already shows that there is more variability in the main peak than in the case of the non-sorbing tracers (Fig. 5), while variability in the tails is less. Comparing the results of KTH and A21 (small dispersivities), the lower peak (and also slightly higher tail) from A21 are consistent with the slightly higher $D_e$ and $K_d$ values (Table 1). The results from JAEA are intermediate between those of TUL-UJV-CTU and those from KTH and A21, consistent with the intermediate value of dispersivity used by JAEA.

The results from PROGEO show a tall and early peak (taller and earlier than those from TUL, CTU or UJV). The reason for this taller and earlier peak lies in how transversal dispersivity was implemented in the different codes. PROGEO implemented zero transversal dispersivity in the slot for the central case, while the other Czech teams used values ranging from 0.019 m to 0.19 m. This implementation of transversal dispersivity resulted in an increased net diffusion/dispersion coefficient at the slot-rock interface, resulting from averaging (arithmetic mean) of diffusion-dispersion coefficients between the two different domains. As a consequence, there was a corresponding net increase in solute fluxes through the interface, explaining the extra retardation (lower and later peaks) in the results from TUL, CTU and UJV. PROGEO also provided results considering a transversal dispersivity of 0.20 m (dotted line in Fig. 5), which plot together with the curves from the other Czech teams and showing this effect. The initial flatter slope of the tail of the PROGEO results (central case) is given by this same effect combined with a relatively coarse spatial discretization. The transversal dispersion effect was negligible for the non-sorbing tracers.

The results from KAERI are very similar to those from UJV and CTU, with only slightly taller and earlier peaks (Fig. 5a). KAERI also implemented transversal dispersion

in their calculations ($\alpha_L = \alpha_T$). The difference in the first arrival times between the different Czech teams and also KAERI is due to numerical discretization effects (Fig. 5b).

Looking at the tails of the breakthrough curves, the lower tail found in the HTO and $^{36}Cl$ results from UJV cannot be observed here. This is due to the fact that the rock capacity factor is dominated here by sorption, and there is no noticeable effect from the smaller porosities implemented by UJV. The tails of the different curves are all rather similar (Fig. 5b; only the PROGEO central-case results are slightly different), pointing to the very similar response of the models to matrix diffusion and sorption, compared to the large differences in the main peak caused by the different dispersivity values.

(a)

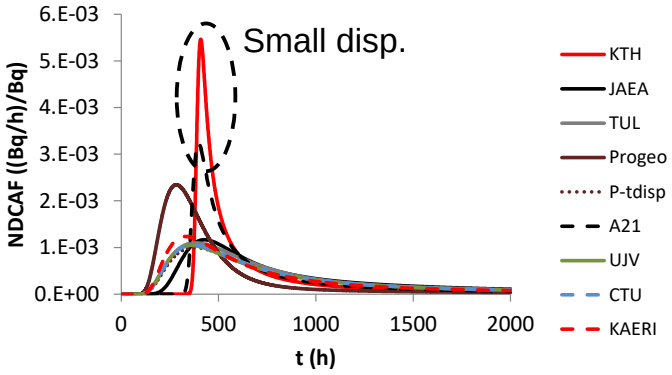


(b)

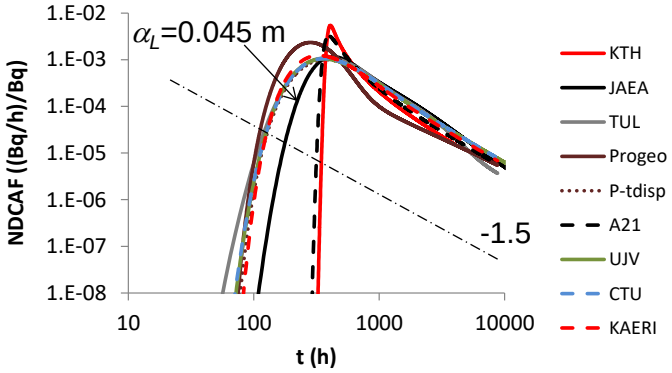


Fig. 5. WPDE-1 model results for $^{22}$Na (NDCAF vs. time). (a) linear – linear scale, (b) log – log scale (a line with a slope of -1.5 is shown for reference). P-tdisp corresponds to the results from PROGEO including transversal dispersivity.

***WPDE-2 (central cases)***

In addition to HTO, $^{36}$Cl and $^{22}$Na, $^{85}$Sr and $^{133}$Ba also were injected in WPDE-2. Modeling results for HTO, $^{36}$Cl and $^{22}$Na were very similar to those from WPDE-1, reflecting only the longer mean water residence time in the experimental borehole (689 h vs. 343 h) due to the smaller flow velocity (10.0 µl/min vs. 20.1 µL/min). As a result, the breakthrough curves shift to later times, as expected. Only the results for $^{85}$Sr and $^{133}$Ba will be shown here. PROGEO did not perform the calculations for WPDE-2.

### $^{85}Sr$

The results from $^{85}$Sr (Fig. 6) show trends which are very similar to those of $^{22}$Na (Fig. 5, WPDE-1). The peak from A21 is shorter than the one from KTH (both teams using small dispersivities; Fig 6a), which is consistent with the slightly higher $D_e$ value used by A21 (Table 1). The peak from TUL is also slightly taller than those from UJV and CTU. The results from KAERI are very similar to those from TUL, with only slightly earlier peak arrival times (Fig. 6a). The results from JAEA are somewhat intermediate between those of TUL-UJV-CTU-KAERI and those from KTH and A21, consistent with the intermediate value of dispersivity used by JAEA. The tails of the different curves are all rather similar, pointing again to the similar response of the models to matrix diffusion and sorption, compared to the large differences in the main peak caused by the different dispersivity values. The difference in the first arrival times between the different Czech teams and also KAERI is due to numerical reasons (Fig. 6b).

(a)

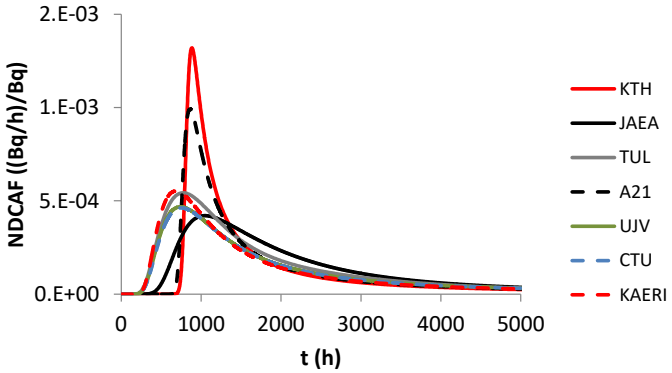


(b)

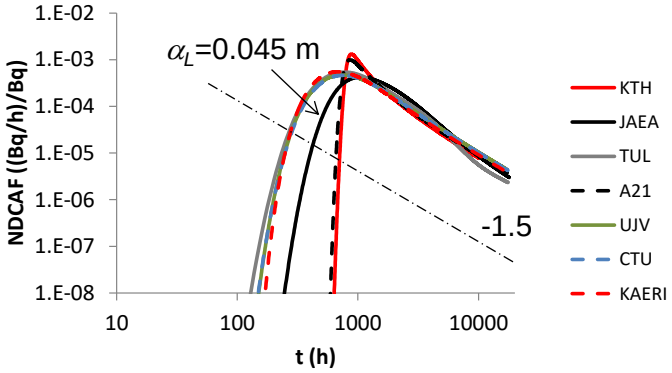


Fig. 6. WPDE-2 model results for $^{85}$Sr (NDCAF vs. time). (a) linear – linear scale, (b) log – log scale (a line with a slope of -1.5 is shown for reference).

*$^{133}$Ba*

This set of the results (Fig. 7), corresponding to the most strongly sorbing tracer, shows the highest variability between the different teams. Concerning the results from the teams considering large dispersivity values, the results from UJV and CTU are practically identical, but those from TUL (central case) show a very tall and late peak and a very flat tail. The three teams used the same parameters (except for the smaller porosities implemented by UJV, which have no effect here). A spatial discretization effect (discretization normal to the slot-rock interface), which can be very important for strongly sorbing tracers, played a significant role. TUL performed a sensitivity study showing that a finer discretization led to earlier first arrival and peak times and shorter peaks (Fig. 7,

TUL-r). The thicknesses of the numerical elements in the rock matrix next to the slot were 0.25 mm and 0.016 mm in the coarse and fine meshes, respectively. The results from KAERI, who performed a convergence check on spatial discretization, are similar to those from TUL (finer discretization).

The results from JAEA show a lower and later peak. The use of a larger dispersivity (0.19 m) shifts the first arrival and peak to earlier times, widening also the breakthrough curve (Fig. 7, JAEA19), but a strong retardation effect caused by the larger $D_e$ value in the BDZ can still be observed. While the $K_d$ value in the BDZ (0.06 $m^3/kg$, Table 1) was comparable to the values used by the other teams, the $D_e$ value ($6\times10^{-13}$ $m^2/s$) was considerably larger, inducing faster tracer uptake by the rock in the BDZ.

The strongly-sorbing nature of the tracer caused very late breakthrough tails, exceeding the calculation times specified in the task (Fig. 7b). A detailed comparison of the tails is therefore not possible.

(a)

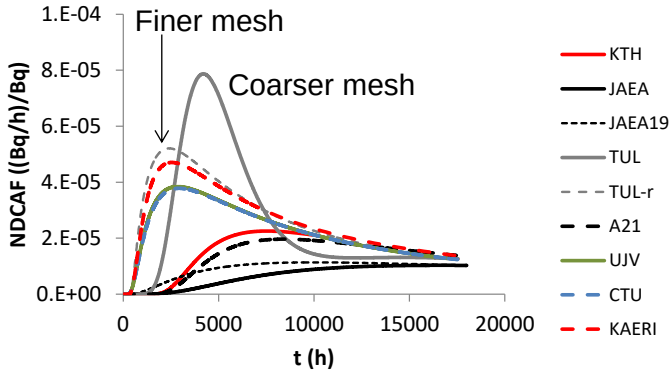


(b)

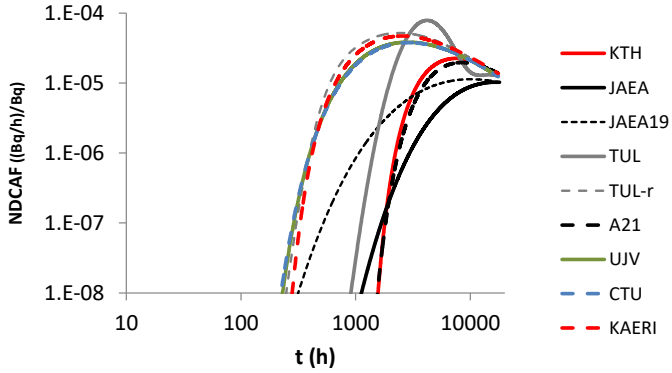


Fig. 7. WPDE-2 model results for $^{133}$Ba (NDCAF vs. time). (a) linear – linear scale, (b) log – log scale. TUL-r corresponds to results from TUL using a refined mesh. JAEA19 coresponds to results from JAEA using a large dispersivity.

***Sensitivity analyses: upper and lower predictions, additional results***

In addition to a central prediction for each tracer, modeling teams were asked to present upper and lower bounds for their breakthrough curves. Additional results from further sensitivity studies or alternative model concepts could also be presented.[13] A summary of these results is reported here.

Conerning upper and lower bounds for the calculated breakthrough curves, the following results were provided:

- KTH provided upper and lower curves for the different tracers based on variations in the value of the Materials Property Group ($MPG = \varepsilon(D_p R)^{0.5} = (D_e \alpha)^{0.5}$), where

$R$ is the retardation factor and $\alpha$ is the rock capacity factor. The value of *MPG* was multiplied and divided by 3.15 to obtain upper and lower curves for each tracer.

- JAEA presented upper and lower curves for each tracer based on the uncertainties (ranges of values) in the supporting experimental data (sorption and diffusion parameters). Single upper and lower curves were those resulting from the changes in the parameter having the largest effect in the results.
- TUL and UJV reported upper and lower curves for each tracer and for each parameter examined, based on the uncertainties (ranges of values) in the supporting experimental data. The parameters examined were $\alpha_L$ (0.1, 0.19, 0.28 m), $\varepsilon$, $K_d$ and $D_e$ for the two rock types included in the models (VGN and PGR).
- CTU provided single upper and lower curves based on the uncertainties (ranges of values) in the supporting experimental data. The upper/lower predictions report the maximum/minimum of all calculated breakthrough curves at a given time.
- A21 provided upper and lower curves for each tracer by considering large and small values of both $D_e$ and $\varepsilon$, keeping their ratio ($D_e/\varepsilon = D_p$) constant.
- KAERI presented upper and lower curves for each tracer based on the uncertainties (ranges of values) in the supporting experimental data ($D_e$, $K_d$). Single upper and lower curves were those resulting from the changes in the parameter having the largest effect in the results.

As an example, results from CTU (single upper and lower curves for HTO and $^{133}$Ba in WPDE-2) are shown in Fig. 8. The curves show the expected potential variability according to the ranges of values for porosity, $D_e$ and $K_d$ for the different tracers in the

supporting experimental data (see supplemental material). The results indicate a larger potential variability in the tails for non-sorbing tracers, as actually observed when comparing the results from the different teams (central cases, Figs. 2b, 4b, 5b, 6b).

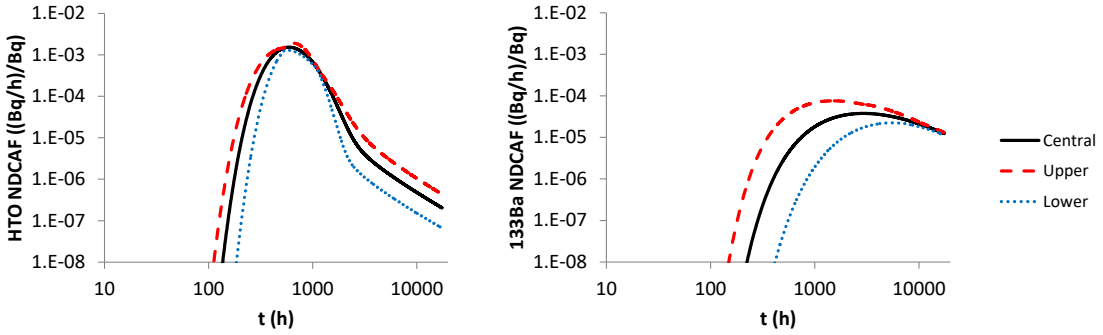


Fig. 8. Calculated breakthrough curves (WPDE-2) from CTU for HTO (left) and $^{133}$Ba (right); central predictions with upper and lower bounds.

Regarding sensitivity analyses and alternative model concepts, the effects of different possible values of longitudinal dispersivities (affecting solute transport in the slot) and of spatial discretization in the rock close to the slot (affecting the results for sorbing tracers) were evaluated by different teams.

Concerning the dispersivities, the following results were reported:

- KTH provided additional results by using different values of dispersion in the slot for HTO (WPDE-1), based on estimated standard deviations for water residence time and aperture of the slot.
- JAEA presented additional calculations considering different values of longitudinal dispersivity in the slot ($\alpha_L$ = 0, 0.045 m, 0.19 m).
- PROGEO reported additional results (WPDE-1) for (a) $\alpha_L$ = 0, 0.1 m, 0.2 m, 0.28 m. Results using zero dispersivity but a variable fracture aperture also resulted in a dispersion effect.

- A21 provided additional results for WPDE-2 (HTO, $^{22}$Na) with $\alpha_L$ = 0.001 m and 0.02 m.
- KAERI provided additional results considering different values of dispersivity ($\alpha_L$ = 0.01$\alpha_{ref}$, 0.1$\alpha_{ref}$, 0.5$\alpha_{ref}$, $\alpha_{ref}$, 1.5$\alpha_{ref}$; $\alpha_{ref}$ = 0.19 m). As an illustration, Figure 9 shows the calculated breakthrough curves for HTO (WPDE-1). As mentioned above, and for non-sorbing or weakly sorbing tracers, small dispersivities result in tall and narrow breakthrough curves with very sharp arrivals, while larger dispersivities result in much shorter and wider curves with very early first arrivals. However, for strongly sorbing tracers, smaller dispersivities result in narrower but also shorter peaks (Fig. 7, JAEA results).

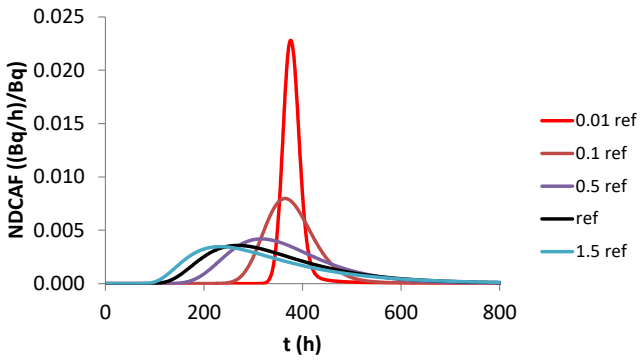


Fig. 9. HTO breakthrough curves (WPDE-1) from KAERI corresponding to different values of longitudinal dispersivity. The reference curve (ref) corresponds to $\alpha_L$ = 0.19 m.

There are some common observations from the teams who used the ranges of values of the reported supporting experimental data (porosities, diffusion coefficients, sorption distribution coefficients) for their sensitivity analyses. The results for the main peak from each team indicated very little sensitivity with respect to the porosity of the rock matrix. Non-sorbing tracers (HTO, $^{36}$Cl) were only significantly affected by the

magnitude of dispersion in the slot, while sorbing tracers were also affected by the values of diffusion and sorption parameters.

TUL, PROGEO and KAERI also studied the effect of spatial discretization on the results for sorbing tracers. Discretization normal to the direction of flow only had an important effect for strongly sorbing tracers. Figure 10 shows the results from KAERI for $^{133}$Ba, showing that a finer discretization results in shorter peaks with erlier first arrival and peak times. It should be noted that the results reported by TUL in their central prediction (Fig. 7) correspond to their coarser mesh, explaining the large difference with the results from other teams.

Additionally, JAEA proposed an alternative conceptual model addressing potential heterogeneous flow in the annular slot. This model case included two different flow channels (10% of the slot with 3 times the average flow velocity and 90% of the slot with 0.78 times the average flow velocity), resulting from potential geometric irregularities in the annulus. The results (Fig. 11, WPDE-2) show the formation of double peaks corresponding to the two channels. These peaks overlap for the strongly sorbing $^{133}$Ba.

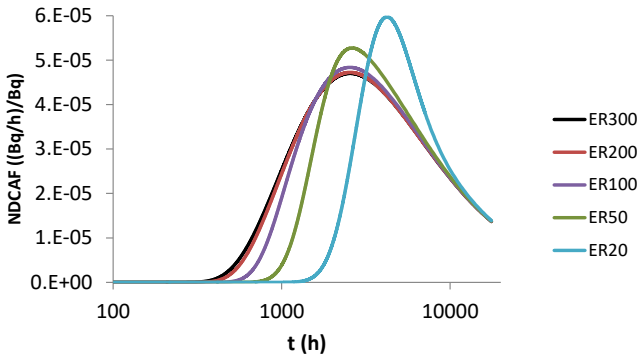


Fig. 10. $^{133}$Ba breakthrough curves (WPDE-2) from KAERI corresponding to different spatial discretizations normal to the direction of flow. All calculations performed with 50 layers of numerical elements in the rock matrix (72 mm thick). ER300 means that the elements next to the slot-matrix interface are 300 times thinner than those at the outer end of the radial domain (72 mm into the rock matrix).

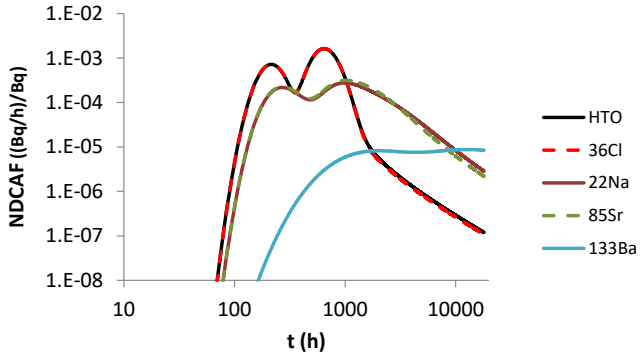


Fig. 11. Breakthrough curves (WPDE-2) from JAEA considering channeling in the slot. The curves for HTO and $^{36}$Cl, and also those for $^{22}$Na and $^{85}$Sr, are practically identical.

## Experimental results

As mentioned in the introduction, this was a blind modeling exercise and the different teams did not have access to the experimental results. However, and for the sake of completeness, the measured breakthrough curves were finally also compared with the model predictions. Figures S1, S2 and S3 in the supplemental material show the calculated breakthrough curves together with the measured experimental data (all in terms of NDCAF vs. time). Measured decay-corrected activities at the outlet (Bq/g) were multiplied by the flow rate and divided by the injected activity to obtain NDCAF.

Activities were measured in water samples for all tracers. For some of the tracers on-line activities were also measured.

Experimental results tend to show relatively small activities, wide breakthroughs and early first arrivals, which are similar to model results using large dispersivity values. However, breakthroughs are always very sharp (very rapid increases in activity) and show at least two well defined peaks, which suggest the existence of multiple flow paths or channels in the slot, with very small dispersivities in each channel (causing the very sharp breakthroughs). Also, experimental results for the non-sorbing tracers (HTO, $^{36}Cl$) show tails with relatively low activities compared with modeling results. Slightly smaller diffusion coefficients and/or porosities may apply to these experimental conditions.

Experimental results for $^{22}Na$ and $^{85}Sr$ show tall and early tracer peaks together with rapid activity drops in the tails of the curves. These features seem to indicate that these tracers sorb less strongly than expected from the reported supporting experimental data (distribution coefficients), or that they diffuse more slowly than expected in the rock matrix. Experimental results for $^{133}Ba$ also show early peaks, although more consistent with the results from the teams assuming large dispersivities (ca. 0.2 m) in the slot.

An additional feature of the measured breakthrough curves is that the first main tracer peak is taller in WPDE-1, while the second main peak is taller in WPDE-2. This feature could indicate heterogeneity with respect to diffusion/retention properties or channel geometries. Different flow geometries in WPDE-1 and WPDE-2 are also a possibility.

**Summary and conclusions**

Purely predictive calculations for a field matrix-diffusion experiment (REPRO WPDE) were performed within the SKB GWFTS Task Force. Tracer breakthrough curves, corresponding to tracer pulse injection, had to be calculated. The different teams had access to supporting experimental information concerning porosities, diffusion coefficients and sorption parameters for the rock matrix. They were free to use different model approaches and use different transport and retention parameters based on the supporting experimental data.

A first conclusion is that even if the objective of the exercise was to focus on matrix diffusion under in situ conditions, the modeling results were finally sensitive to the assumed magnitude of dispersion in the slot, which is related to the flow of water and not to transport and retention in the rock matrix. Modeling teams considered different conceptual models of flow and transport in the fracture: Taylor dispersion, dispersion length (typically $1/10^{th}$ of the path length), variable apertures and multiple flow paths. These different concepts significantly influenced the resulting dispersion in the fracture. On the other hand, differences in the conceptualization of diffusion and sorption in the rock were only minor. Advection and dispersion have a strong effect on the main peak of the tracer breakthrough curves, while the tails reflect back-diffusion from the rock matrix after the end of the tracer pulses. Given that the time scales for advection and matrix diffusion were considerably different, the two parts of the curves are decoupled and the tails of the curves reflect only tracer diffusion and retention in the rock matrix.

Regarding the sensitivity analyses conducted by the different teams (upper and lower bounds of the breakthrough curves, additional results), they confirmed the large sensitivity of the results for the main peak to dispersion. However, the different dispersivity values did not affect the tails of the breakthrough curves. Also concerning the main peak, and considering the ranges of values of the reported supporting

experimental data (porosities, diffusion coefficients, sorption distribution coefficients), results from each team indicated very little sensitivity to the porosity of the rock matrix. Non-sorbing tracers (HTO, $^{36}Cl$) were only significantly affected by the magnitude of dispersion in the slot, while sorbing tracers were also affected by the values of diffusion and sorption parameters. At the same time, and according to those ranges of values, the expected potential variability in the tails of the breakthrough curves was larger for non-sorbing tracers.

The thickness of rock matrix considered in the models is an important parameter affecting the results for non-sorbing tracers, since these conservative tracers can move a considerable distance into the rock. Also, the assumption or not of potentially reduced porosities and diffusion coefficients for $^{36}Cl$ (anion exclusion) affects the tails of the breakthrough curves.

Very significant differences have been observed between the models in the results for the most strongly sorbing tracer ($^{133}Ba$). Spatial discretization plays an important role here. Checking the convergence of the results with respect to spatial discretization, which is always a basic modeling practice, is particularly important in the case of strongly sorbing species.

Other issues observed in the results include a numerical effect arising from the implementation of transversal dispersivity in the slot, which translates into additional retardation for sorbing tracers. The reason for this effect is the averaging of transport properties at the slot-matrix interface. Harmonic means of transport properties, instead of arithmetic means, should be used at those interfaces. Also, slightly different positions of the peaks and small differences in first arrival times can be due to numerical discretization effects.

In summary, the comparison between the different sets of modeling results, reflecting the use of different codes and modeling approaches, has provided important information concerning the reasons for the differences in the results, which can eventually be relevant for performance assessment calculations of potential deep geological disposal of radioactive waste. The importance of contrasting different concepts and tools (including analytical solutions) has been shown. The effects of errors when implementing parameter values in the codes are also reflected in the results.

This study has focussed on the differences between the blind predictive models used to simulate the experiments. A full discussion of the experimental results and their interpretation is provided in two POSIVA reports.[10,11] For the sake of completeness, the models have also been finally compared to the measured experimental breakthroughs. Experimental results tend to show relatively small activities, wide breakthroughs and early first arrivals, which are similar to model results using large dispersivity values. However, breakthroughs are always very sharp and show at least two well defined peaks, which suggest the existence of multiple flow paths or channels in the slot, with very small dispersivities in each channel.

**Acknowledgements**

The authors are grateful to Martin Löfgren and Kersti Nilsson as Principal Investigators of Task 9 in the GWFTS Task Force. The helpful comments from Mark Elert, Kersti Nilsson and Antti Poteri, and the discussions with the whole Task 9 team, are also thankfully acknowledged. Funding was provided through the Task Force partner organizations participating in this modeling exercise (SKB, Sweden; SURAO, Czech Republic; KAERI, Republic of Korea; NUMO and JAEA; Japan). IDAEA-CSIC is a

Center of Excelence Severo Ochoa (Spanish Ministry of Science and Innovation, Project CEX2018-000794-S).

## References

1. J. HADERMANN, and W. HEER, "The Grimsel (Switzerland) Migration Experiment: Integrating Field Experiments, Laboratory Investigations and Modelling," *Journal of Contaminant Hydrology*, **21**, 87-100 (1996); http://10.1016/0169-7722(95)00035-6.

2. P. M. JARDINE et al., "Quantifying Diffusive Mass Transfer in Fractured Shale Bedrock," *Water Resources Research*, **35**, 2015-2030 (1999); http://10.1029/1999WR900043.

3. I. NERETNIEKS, "A Stochastic Multi-Channel Model for Solute Transport - Analysis of Tracer Tests in Fractured Rock," *Journal of Contaminant Hydrology*, **55**, 175-211 (2002); http://10.1016/S0169-7722(01)00195-4.

4. M. MAZUREK, A. JAKOB, and P. BOSSART, "Solute Transport in Crystalline Rocks at Äspö — I: Geological Basis and Model Calibration," *Journal of Contaminant Hydrology*, **61**, 157-174 (2003); http://10.1016/S0169-7722(02)00137-7.

5. A. JAKOB, M. MAZUREK, and W. HEER, "Solute Transport in Crystalline Rocks at Äspö — II: Blind Predictions, Inverse Modelling and Lessons Learnt from Test STT1," *Journal of Contaminant Hydrology*, **61**, 175-190 (2003); http://10.1016/S0169-7722(02)00136-5.

6. A. POLAK et al., "Chemical Diffusion Between a Fracture and the Surrounding Matrix: Measurement by Computed Tomography and Modeling," *Water Resources Research*, **39**, 1106 (2003); http://10.1029/2001WR000813.

7. Q. ZHOU et al., “Field-Scale Effective Matrix Diffusion Coefficient for Fractured Rock: Results from Literature Survey,” *Journal of Contaminant Hydrology*, **93**, 161-187 (2007); http://10.1016/j.jconhyd.2007.02.002.

8. D. HODGKINSON et al., “An Overview of Task 6 of the Äspö Task Force: Modelling Groundwater and Solute Transport: Improved Understanding of Radionuclide Transport in Fractured Rock,” *Hydrogeology Journal*, **17**, 1035-1049 (2009); http://10.1007/s10040-008-0416-9.

9. V. CVETKOVIC et al., “Inference of Retention Time from Tracer Tests in Crystalline Rock,” *Water Resources Research*, **56**, e2019WR025266 (2020); http://10.1029/2019WR025266.

10. A. POTERI et al., “The First Matrix Diffusion Experiment in the Water Phase of the REPRO Project: WPDE 1,” POSIVA Working Report 2017-23, POSIVA, Eurajoki, Finland (2018).

11. A. POTERI et al., “The Second Matrix Diffusion Experiment in the Water Phase of the REPRO Project: WPDE 2,” POSIVA Working Report 2017-24. POSIVA, Eurajoki, Finland (2018).

12. M. LÖFGREN, and K. NILSSON, “SKB Task Description of Task 9A – Modelling of REPRO Experiments WPDE-1 and WPDE-2. Task 9 of SKB Task Force GWFTS – Increasing the Realism in Solute Transport Modelling Based on the Field Experiments REPRO and LTDE-SD,” SKB Report P-17-18, SKB, Solna, Sweden (2019).

13. J. M. SOLER et al., “Evaluation and Modelling Report of Task 9A Based on Comparisons and Analyses of Predictive Modelling Results for the REPRO WPDE experiments. Task 9 of SKB Task Force GWFTS – Increasing the Realism in Solute Transport Modelling Based on the Field Experiments REPRO and LTDE-SD,” SKB Report R-17-10, SKB, Solna, Sweden (2019).

14. GOLDSIM TECHNOLOGY GROUP, “User’s Guide, GoldSim, Probabilistic Simulation Environment,” GoldSim Technology Group, Issaquah, WA, USA (2018).

15. J. BŘEZINA et al., “Flow123d, Version 2.2.1, User Guide and Input Reference,” Technical university of Liberec, Faculty of Mechatronics, Informatics and Interdisciplinary Studies, Liberec, Czech Republic (2018).

16. C. ZHENG, “MT3DMS v5.3 Supplemental User’s Guide. Technical Report to the US Army Engineer Research and Development Center,” Department of Geological Sciences, University of Alabama, Tuscaloosa, AL, USA (2010).

17. G. HAMMOND, P. LICHTNER, and R. MILLS, “Evaluating the Performance of Parallel Subsurface Simulators: An Illustrative Example with PFLOTRAN,” *Water Resources Research*, **50**, 208-228 (2014); http://10.1002/2012WR013483.

18. Q. LI et al., “COMSOL Multiphysics: A Novel Approach to Ground Water Modeling,” *Groundwater*, **47**, 480-487 (2009); http://10.1111/j.1745-6584.2009.00584.x.

19. J. PERKO, S. C. SEETHARAM, and D. MALLANTS, “Simulation Tools Used in Long-Term Radiological Safety Assessments. Project Near Surface Disposal of Category A Waste at Dessel,” NIROND-TR 2008-11 E, ONDRAF/NIRAS, Brussels, Belgium (2009).

20. A. JAKOB, and J. HADERMANN, “INTRAVAL Finnsjon Test. Modelling Results for Some Tracer Experiments,” Nagra Technical Report 94-21, Nagra, Wettingen, Switzerland (1994).

21. S. PAINTER, V. CVETKOVIC, and J.-O. SELROOS, “Transport and Retention in Fractured Rock: Consequences of a Power-Law Distribution for Fracture Lengths”, *Physical Review E*, **57**, 6917-6922 (1998); http://10.1103/PhysRevE.57.6917.

22. V. CVETKOVIC, “Diffusion-Controlled Tracer Retention in Crystalline Rock on the Field Scale,” *Geophysical Research Letters* **37**, L13401 (2010); http://10.1029/2010GL043445.

23. D. TANG, E. FRIND, and E. A. SUDICKY, “Contaminant Transport in Fractured Porous Media: Analytical Solution for a Single Fracture,” *Water Resources Research*, **17**, 555–564 (1981); http://10.1029/WR017i003p00555.

24. E. A. SUDICKY, and E. FRIND, “Contaminant Transport in Fractured Porous Media: Analytical Solution for a System of Parallel Fractures,” *Water Resources Research*, **18**, 1634–1642 (1982); http://10.1029/WR018i006p01634.

25. C. I. STEEFEL et al., “Reactive Transport Codes for Subsurface Environmental Simulation,” *Computational Geosciences*, **19,** 445-478 (2015); http://10.1007/s10596-014-9443-x.

26. C. I. STEEFEL, and S. MOLINS, “CrunchFlow. Software for Modeling Multicomponent Reactive Flow and Transport. User’s Manual,” Lawrence Berkeley National Laboratory. Berkeley, CA, USA (2016).

27. I. NERETNIEKS, and L. MORENO, “Prediction of Some In Situ Tracer Tests with Sorbing Tracers Using Independent Data,” *Journal of Contaminant Hydrology*, **61**, 351-360 (2003); http://10.1016/S0169-7722(02)00123-7.

Figures S1 to S3 below show the results (breakthrough curves) from the predictive models together with the experimental measurements. Results are shown in both linear-linear and log-log scales.

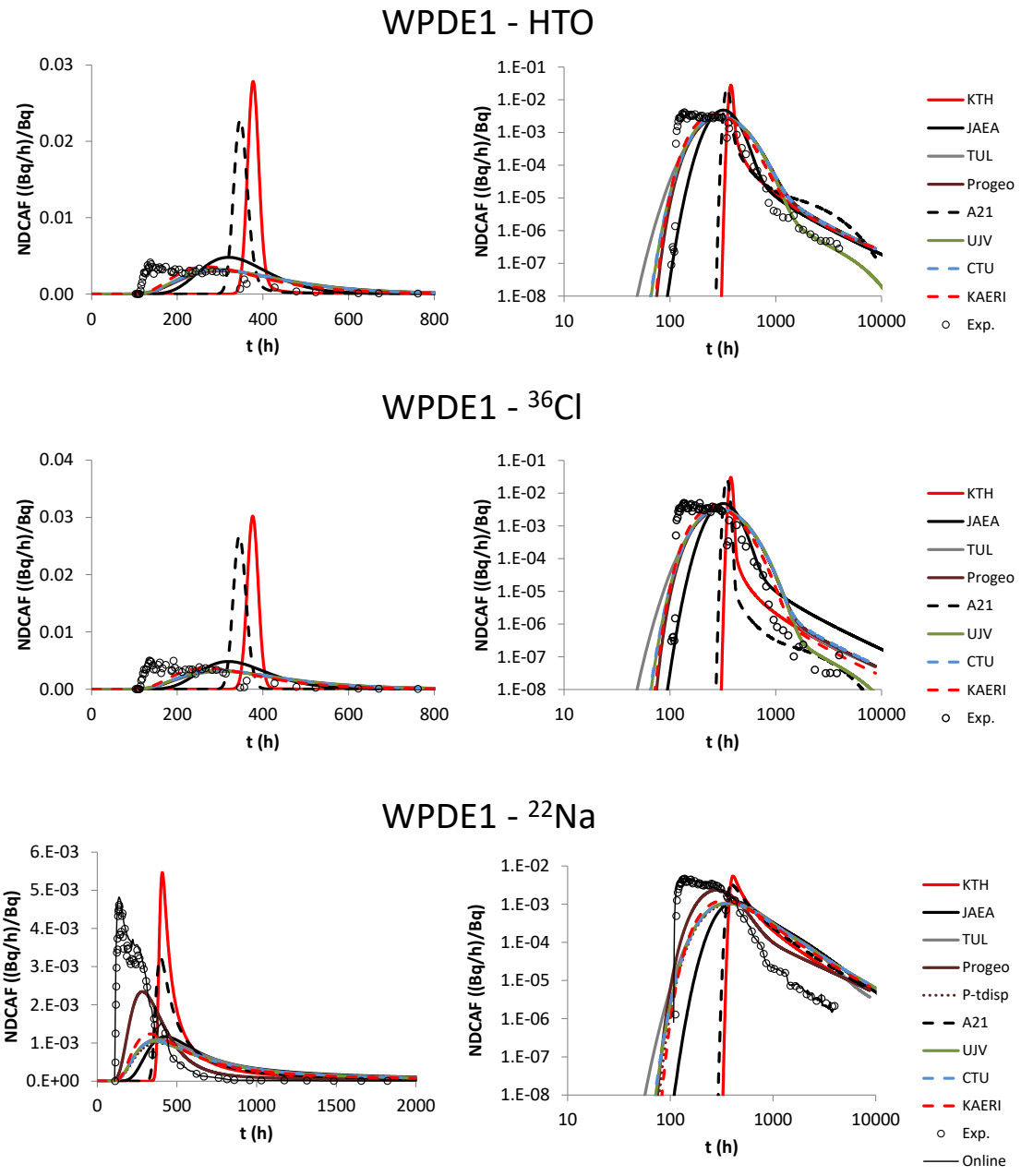


**Figure S1.** Model and experimental breakthrough curves (NDCAF vs. time) for WPDE-1. Small circles correspond to activities measured in water samples. The thin black line ($^{22}$Na) corresponds to online measurement.

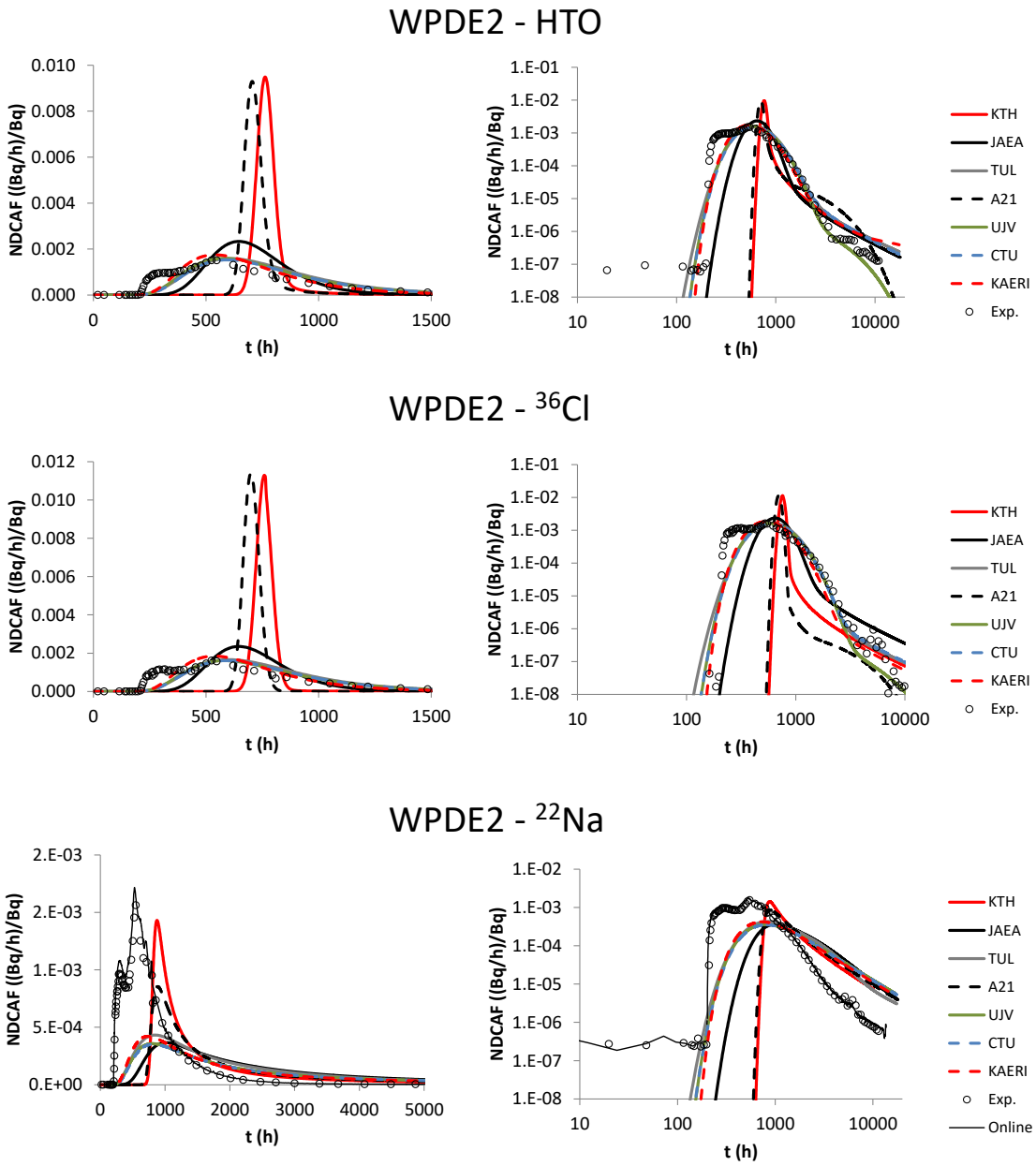


**Figure S2.** Model and experimental breakthrough curves (NDCAF vs. time) for WPDE-2. Small circles correspond to activities measured in water samples. The thin black line ($^{22}$Na) corresponds to online measurement.

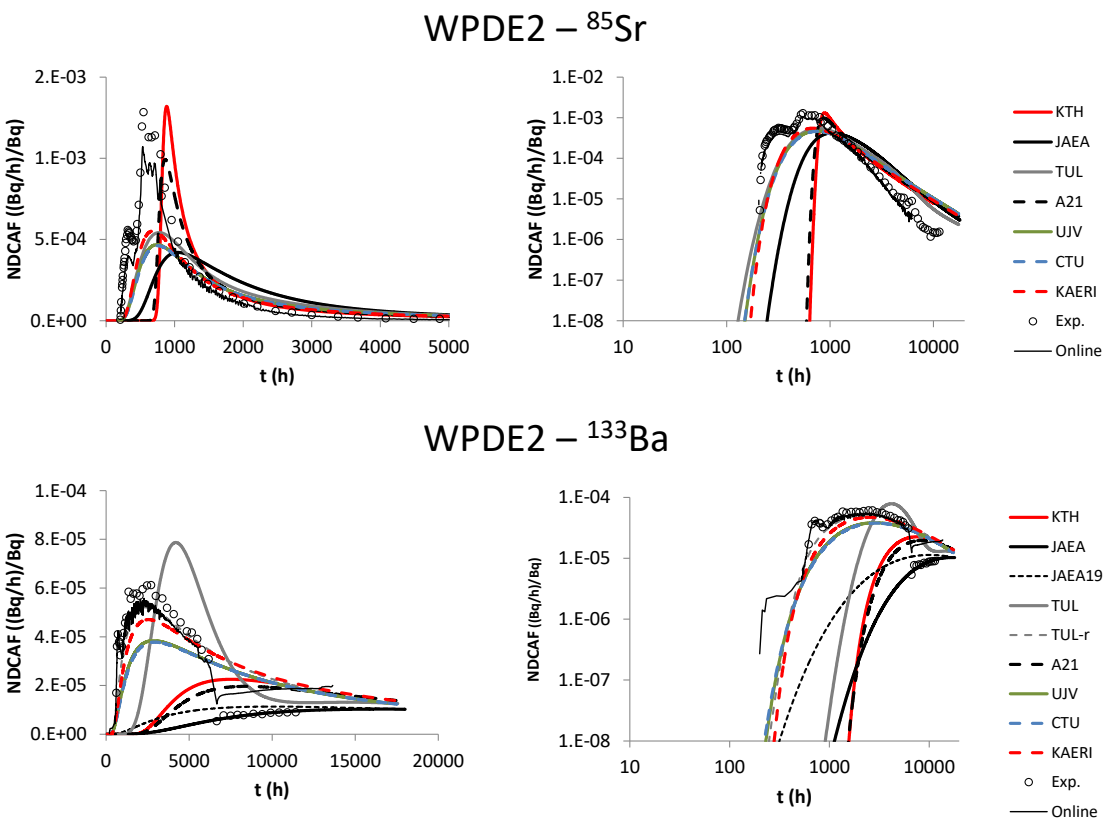


**Figure S3.** Model and experimental breakthrough curves (NDCAF vs. time) for WPDE-2. Small circles correspond to activities measured in water samples. The thin black lines ($^{85}$Sr, $^{133}$Ba) corresponds to online measurements.

Tables S1 to S3 below provide a summary of the laboratory experimental results available to the modeling teams.

**Table S1.** Rock matrix porosities obtained in the REPRO laboratory campaign. Data are reproduced from Ikonen et al. (2015) and, where noted, from Kuva et al. (2015).

| Drillhole | Drillhole lengths (m) | Porosity (%) | Method |
|---|---|---|---|
| ONK-PP323 | 18.02-18.07 | 0.82 ± 0.13 | Ar-pycnometry (Kuva et al. 2015) |
| ONK-PP323 | 18.12-18.15 | 2.7 ± 0.3 | Ar-pycnometry (Kuva et al. 2015) |
| ONK-PP323 | 18.71-18.74 | 1.20 ± 0.12 | $^{14}$C-PMMA autoradiography |
| ONK-PP323 | 18.75-18.78 | 0.64 ± 0.16<br>0.40 ± 0.04 | Water gravimetry<br>$^{14}$C-PMMA autoradiography |
| ONK-PP323 | 18.78-18.83 | 0.85 ± 0.23 | Water gravimetry |
| ONK-PP323 | 18.83-18.89 | 1.24 ± 0.14 | Ar-pycnometry |
| ONK-PP323 | 19.02-19.07 | 0.65 ± 0.05 | Ar-pycnometry |
| ONK-PP323 | 19.07-19.10 | 0.45 ± 0.12<br>0.50 ± 0.05 | Water gravimetry<br>$^{14}$C-PMMA autoradiography |
| ONK-PP323 | 19.10-19.12 | 0.70 ± 0.07 | $^{14}$C-PMMA autoradiography |
| ONK-PP323 | 19.12-19.17 | 0.30 ± 0.03 | $^{14}$C-PMMA autoradiography |
| ONK-PP323 | 20.89-20.91 | 0.19 ± 0.08 | Ar-pycnometry (Kuva et al. 2015) |
| ONK-PP318 | 13.92-13.95 | 0.6 ± 0.3 | Ar-pycnometry (Kuva et al. 2015) |
| ONK-PP318 | 13.97-14.02 | 0.63 ± 0.05 | Ar-pycnometry (Kuva et al. 2015) |
| ONK-PP318 | 15.62-15.65 | 0.30 ± 0.04 | $^{14}$C-PMMA autoradiography |
| ONK-PP318 | 15.65-15.66 | 0.70 ± 0.07 | $^{14}$C-PMMA autoradiography |
| ONK-PP318 | 15.66-15.69 | 0.42 ± 0.12<br>0.50 ± 0.05 | Water gravimetry<br>PMMA autoradiography |
| ONK-PP318 | 15.69-15.74 | 0.49 ± 0.14 | Water gravimetry |
| ONK-PP318 | 15.74-15.79 | 0.44 ± 0.05 | Ar-pycnometry |

**Table S2.** Rock matrix effective diffusivity obtained by water phase through-diffusion experiments at Helsinki University (unpublished data).

| Drillhole | Drillhole lengths (m) | Tracer | Effective diffusivity, $D_e$ ($m^2/s$) | Rock capacity factor, $\alpha$ (–) |
|---|---|---|---|---|
| ONK-PP323 | 18.89 – 18.94 | HTO | $(2.5 \pm 0.3)\cdot10^{-13}$ | 0.0070 ± 0.0005 |
| ONK-PP323 | 18.94 – 18.96 | HTO<br>Cl-36 | $(1.6 \pm 0.3)\cdot10^{-13}$<br>$(0.05 \pm 0.03)\cdot10^{-13}$ | 0.011 ± 0.001<br>0.0002 ± 0.0005 |
| ONK-PP323 | 18.96 – 18.98 | HTO<br>Cl-36 | $(1.4 \pm 0.2)\cdot10^{-13}$<br>$(0.05 \pm 0.03)\cdot10^{-13}$ | 0.011 ± 0.001<br>0.00015 ± 0.0005 |
| ONK-PP318 | 15.79 – 15.84 | HTO<br>Cl-36 | $(5.7 \pm 0.6)\cdot10^{-13}$<br>$(5 \pm 1)\cdot10^{-13}$ | 0.013 ± 0.001<br>0.013 ± 0.002 |

**Table S3.** Measured porosities, effective diffusion coefficients, and permeabilities, as well as rock types of the REPRO samples. Error estimates are given as ±1 σ. Data are reproduced from Kuva et al. (2015, Table 2) but sample labelling has been updated and sample foliation is added for borehole ONK PP323-PP327. PGR: Pegmatitic granite. VGN: Veined gneiss.

| Sample | Porosity ε [%] | Gas diffusion $D_e \times 10^{-9}$ ($m^2/s$) | Permeability $k \times 10^{-19}$ ($m^2$) | Rock type | Foliation |
|---|---|---|---|---|---|
| ONK-PP318 13.92-13.95 | 0.6 ± 0.3 | 8.2 ± 0.8 | 860 ± 70 | PGR | - |
| ONK-PP318 13.97-14.02 | 0.63 ± 0.05 | 3.2 ± 0.6 | 64 ± 1 | PGR | - |
| ONK-PP318 15.74-15.79 | 0.44 ± 0.14 | 5.7 ± 0.5 | 5.9 ± 0.2 | PGR | - |
| ONK-PP318 16.87-16.92 | 0.70 ± 0.05 | 6.7 ± 0.7 | 9 ± 1 | VGN | - |
| ONK-PP319 9.16-9.21 | 0.34 ± 0.14 | 2.0 ± 0.2 | 1.3 ± 0.2 | VGN | - |
| ONK-PP319 9.47-9.52 | 2.4 ± 0.2 | 1.4 ± 0.3 | 6 ± 1 | VGN | - |
| ONK-PP319 12.46-12.51 | 0.77 ± 0.15 | 2.8 ± 0.2 | 1.1 ± 0.1 | VGN | - |
| ONK-PP319 12.70-12.75 | 0.6 ± 0.14 | 3.8 ± 0.5 | 49 ± 5 | VGN | - |
| ONK-PP321 10.26-10.31 | 0.55 ± 0.14 | 1.9 ± 0.7 | 39 ± 1 | VGN | - |
| ONK-PP323 18.02-18.07 | 0.82 ± 0.13 | 3 ± 1 | 11.3 ± 0.1 | VGN | ⊥ |
| ONK-PP323 18.12-18.15 | 2.7 ± 0.3 | 5.4 ± 0.5 | 53 ± 5 | VGN | ⊥ |
| ONK-PP323 18.83-18.89 | 1.24 ± 0.14 | 0.58 ± 0.05 | 0.2 ± 0.1 | VGN | ⊥ |
| ONK-PP323 19.02-19.07 | 0.7 ± 0.2 | 0.50 ± 0.05 | 0.14 ± 0.02 | VGN | ⊥ |
| ONK-PP323 20.89-20.91 | 0.19 ± 0.08 | 0.75 ± 0.1 | 0.9 ± 0.1 | VGN | ⊥ |
| ONK-PP324 11.49-11.51 | 1.02 ± 0.05 | 0.8 ± 0.1 | 3.6 ± 0.4 | VGN | ‖ |
| ONK-PP326 11.42-11.44 | 2.9 ± 0.1 | 1.4 ± 0.1 | 2.0 ± 0.2 | VGN | ‖ |
| ONK-PP326 11.72-11.74 | 0.68 ± 0.08 | 1.1 ± 0.1 | 9.5 ± 0.2 | VGN | ‖ |
| ONK-PP327 12.05-12.07 | 0.7 ± 0.1 | 1.2 ± 0.1 | 0.2 ± 0.1 | VGN | ‖ |

**Table S4.** Sorption partitioning coefficients obtained in batch experiments on crushed rock of different size fractions by Helsinki University (unpublished data). Uncertainty estimates represent one standard deviation.

| Radionuclide | Rock type | Sorption partitioning coefficients ($m^3/kg$) |
|---|---|---|
| Na-22 | Veined gneiss | 0.0013 ± 0.0003 |
| | Pegmatitic granite | 0.0008 ± 0.0003 |
| Sr-85 | Veined gneiss | 0.0011 ± 0.0003 |
| | Pegmatitic granite | 0.0011 ± 0.0003 |
| Ba-133 | Veined gneiss | 0.06 ± 0.02 |
| | Pegmatitic granite | 0.08 ± 0.02 |

## References

Ikonen J, Sammaljärvi J, Siitari-Kauppi M, Voutilainen M, Lindberg A, Kuva J, Timonen J (2015) Investigation of Rock Matrix Retention Properties Supporting Laboratory Studies I: Mineralogy, Porosity, and Pore Structure. POSIVA Working Report 2014-68, Posiva Oy, Finland.

Kuva J, Voutilainen M, Kekäläinen P, Siitari-Kauppi M, Timonen J, Koskinen L (2015) Gas phase measurements of porosity, diffusion coefficient, and permeability in rock samples from Olkiluoto bedrock, Finland. Transport in Porous Media 107, 187-204.